Temperature-Induced Structure Transformation from $Co_{0.85}Se$ to Orthorhombic Phase $CoSe_2$ Realizing Enhanced Hydrogen Evolution Catalysis

Jing Bai, Yechen Wang, Yange Wang, Tiantian Zhang, Gang Dong, Dongsheng Geng,* and Dongjie Zhao*

Read Online

ACCESS | Metrics & More | Article Recommendations | Supporting Information

ABSTRACT: Transition-metal chalcogenides (TMC) have been widely studied as active electrocatalysts toward the hydrogen evolution reaction due to their suitable d-electron configuration and relatively high electrical conductivity. Herein, we develop a feasible method to synthesize an orthorhombic phase of $CoSe_2$ (o-$CoSe_2$) from the regeneration of $Co_{0.85}Se$, where the temperature plays a key role in controlling the structure transformation. To the best of our knowledge, this is the first report about this synthetic route for o-$CoSe_2$. The resulting o-$CoSe_2$ catalysts exhibit enhanced hydrogen evolution reaction performance with an overpotential of 220 mV to reach 10 mA cm^{-2} in 1.0 M KOH. Density functional theory calculations further reveal that the change in the Gibbs free energy of hydrogen, water adsorption energy, and the downshifted d-band center make o-$CoSe_2$ more suitable for accelerating the HER process.
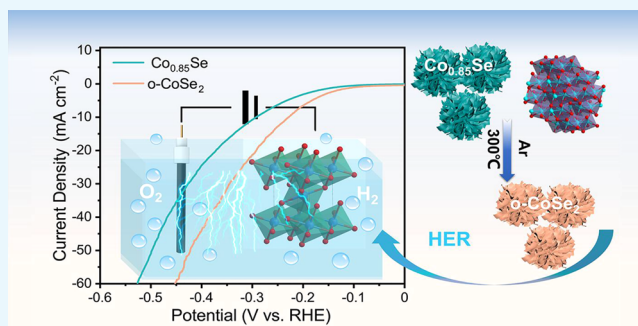
1. INTRODUCTION

On account of the global energy crisis and environmental issues, hydrogen has been extensively considered to hold great promise for the development of alternative and sustainable energy sources to replace fossil fuels.[1−4] Water electrolysis is one attractive technology to produce hydrogen (H_2) from renewable sources.[5−7] To achieve the large-scale and efficient production of H_2, it is necessary and vital to develop high-performance electrocatalysts toward the hydrogen evolution reaction (HER).[8−10] Up to now, noble metals (such as Pt and Ru) have been deemed to be the state of the art electrocatalysts for HER, but their high cost and scarcity have severely hindered the widespread industrial application.[11−13] Thus, it is desirable to seek low-cost non-noble-metal catalysts to boost the HER process efficiently.

As one of the attractive alternatives, transition-metal chalcogenides (TMC) have been widely investigated as highly active electrocatalysts in many studies due to their suitable d-electron configuration and relatively high electrical conductivity.[14−18] Among them, cobalt selenides can be considered to be a special case due to their unique synthesis method of structure transformation engineering. For instance, there are two phases of $CoSe_2$, one is a cubic phase (c-$CoSe_2$) and the other is an orthorhombic phase (o-$CoSe_2$).[19,20] It has been confirmed in Xie's report that the realization of a structure transformation from o-$CoSe_2$ to c-$CoSe_2$ can enhance alkaline HER performance.[21] The obtained c-$CoSe_2$/C needs an over-

potential of only 190 mV to achieve a current density of 10 mA cm^{-2}, while a higher overpotential of 270 mV is needed for o-$CoSe_2$/C. Density functional theory (DFT) calculations reveal that both the change in Gibbs free energy (ΔG_{H*}) of c-$CoSe_2$ and the water adsorption energy are optimized, which can strengthen the electrocatalytic activity of the catalyst for HER. Structure transformation engineering has also been achieved by controlling the level of P-doping, and the o-$CoSe_2$ induced by doping has shown HER activity superior to that of the original c-$CoSe_2$.[22] The P-doped o-$CoSe_2$ catalyst possesses an optimized electronic structure and local coordination environment after the structure transformation, which leads to a substantial energetic benefit for the HER. Furthermore, a structure transformation has been realized from o-$CoSe_2$ to m-Co_3Se_4 (monoclinic phase Co_3Se_4), attributed to the addition of Cu(II) ions. The resulting Cu-14-Co_3Se_4/GC catalyst with a trace amount of Cu shows enhanced HER, OER, and ORR activities.[23] Therefore, an in-depth investigation into the structural change and the corresponding
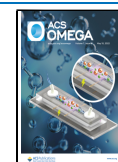
Figure 1. Schematic illustration of o-CoSe$_2$ NSS derived from Co$_{0.85}$Se NSS for the alkaline HER.

electrocatalytic performance of cobalt selenides might be beneficial to design highly efficient catalysts toward HER. Furthermore, the OER activity of o-CoSe$_2$ in some reports has been improved.[24−26] There has been very little research work on o-CoSe$_2$ as an electrocatalyst for the alkaline HER which will impede its further application in water splitting.

Herein, we demonstrate the structural transformation from flowerlike Co$_{0.85}$Se nanosheets (denoted Co$_{0.85}$Se NSS) to o-CoSe$_2$ nanosheets (denoted o-CoSe$_2$ NSS) with an improved alkaline HER performance through a simple heat treatment strategy. DFT calculations suggest that the change from Co$_{0.85}$Se NSS to o-CoSe$_2$ NSS can modulate the intrinsic electronic structure, which can benefit the kinetics of the HER process. As a result, the prepared o-CoSe$_2$ NSS exhibits a better electrocatalytic activity in 1.0 M KOH with an overpotential of 220 mV instead of the 286 mV needed by Co$_{0.85}$Se NSS to reach 10 mA cm^{-2}. This work provides a broader perspective to develop CoSe$_2$ materials with high activity by a simple and controllable structure transformation method.

2. EXPERIMENTAL SECTION

2.1. Synthesis of ZIF-67 Precursor. In a typical process for the synthesis of ZIF-67 (reported in a previous article[24]), 5.85 g of Co(NO$_3$)$_2$·6H$_2$O and 6.16 g of 2-methylimidazole (2-MeIm) were dissolved in 150 mL portions of methanol with continuous stirring until they fully dissolved to become two transparent solutions, denoted A and B. Then solution B was quickly poured into solution A and the mixed solution was stirred for 24 h at room temperature. Finally, a purple product was obtained by filtration with ethanol for several times and dried at 60 °C.

2.2. Synthesis of Co$_{0.85}$Se NNS and o-CoSe$_2$ NNS.
2.2.1. Co$_{0.85}$Se NNS. Co$_{0.85}$Se NNS was obtained by a selenization process using a hydrothermal method. Typically, 50 mg of ZIF-67 powder was poured into 10 mL deionized water and mixed with ultrasound for 10 min. After that, the mixed solution was added to 15 mL deionized water containing sodium selenite (Na$_2$SeO$_3$). Moreover, 2 mL hydrazine hydrate (N$_2$H$_4$·H$_2$O) was added in the above solution with 10 min of stirring. Then the mixed solution was transferred into a 50 mL Teflon-linked steel autoclave and kept at 200 °C for 20 h. The obtained black product was washed several times with deionized water and ethanol, respectively, and then dried at 60 °C.

2.2.2. o-CoSe$_2$ NNS. o-CoSe$_2$ NNS was synthesized by a simple heat treatment. The above Co$_{0.85}$Se NNS product was placed in a tube furnace and annealed at 300 °C at a heating rate of 2 °C min^{-1} for 2 h under an Ar atmosphere.

2.3. Material Characterization. The composition and crystal structure of the obtained products were characterized by X-ray diffraction (XRD, Rigaku Smartlab3 instrument with Cu Kα radiation). The microstructure was investigated by transmission electron microscopy (TEM, JEOL, JEM-2200FS) and scanning electron microscopy (SEM, SUPRA 55, Zeiss). X-ray photoelectron spectroscopy (XPS) was carried out with a PHI 5000 Versa Probe III instrument with an Al Kα X-ray source.

2.4. Electrochemical Measurements. The electrochemical measurements were carried out on an electrochemical workstation (CHI 660E, CH Instruments Inc., Shanghai, China) in a typical three-electrode cell. The as-synthesized products served as the working electrodes, and a Hg/HgO electrode and a graphite rod were used as the reference electrode and the counter electrode, respectively. A 1 M KOH aqueous solution was used as the electrolyte. Polarization curves of HER were measured at a scan rate of 2 mV s^{-1} without iR compensation. Electrochemical impedance spectra (EIS) tests were performed at an overpotential of 275 mV from 100 kHz to 10 mHz. The electrochemical stability was determined by a chronoamperometric test. To evaluate the electrochemical double-layer capacitance (C_{dl}), the cyclic voltammetry (CV) curves were obtained at different scan rates (20−180 mV s^{-1}) in the voltage ranges of −0.1 to 0 V without a Faradaic potential region. The electrochemical active surface area (ECSA) was directly proportional to C_{dl}. All potential measurements were calibrated against the reversible hydrogen electrode (RHE).

2.5. Theoretical Calculations. We used a first-principles method[28,29] to obtain the spin-polarization density functional theory (DFT) calculations within the generalized gradient approximation (GGA) using the Perdew−Burke−Ernzerhof (PBE) formulation.[30] The projector augmented wave (PAW) potentials[31,32] were employed to describe the ionic cores and take valence electrons into account using a plane wave basis set with a cutoff energy of 450 eV. Partial occupancies of the Kohn−Sham orbitals were obtained using the Gaussian smearing method and a width of 0.05 eV. The electronic energy was taken as being self-consistent, while the energy change was smaller than 10^{-6} eV. A geometry optimization was
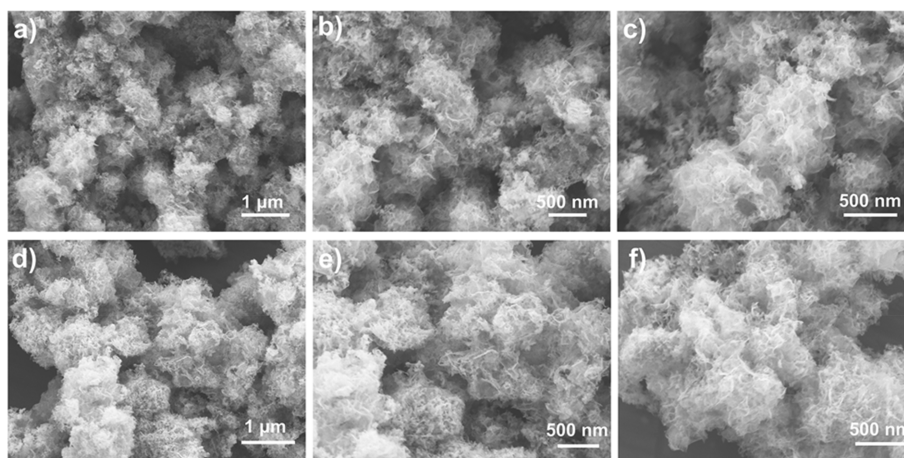
Figure 2. SEM images of (a−c) Co$_{0.85}$Se NSS and (d−f) o-CoSe$_2$ NSS.

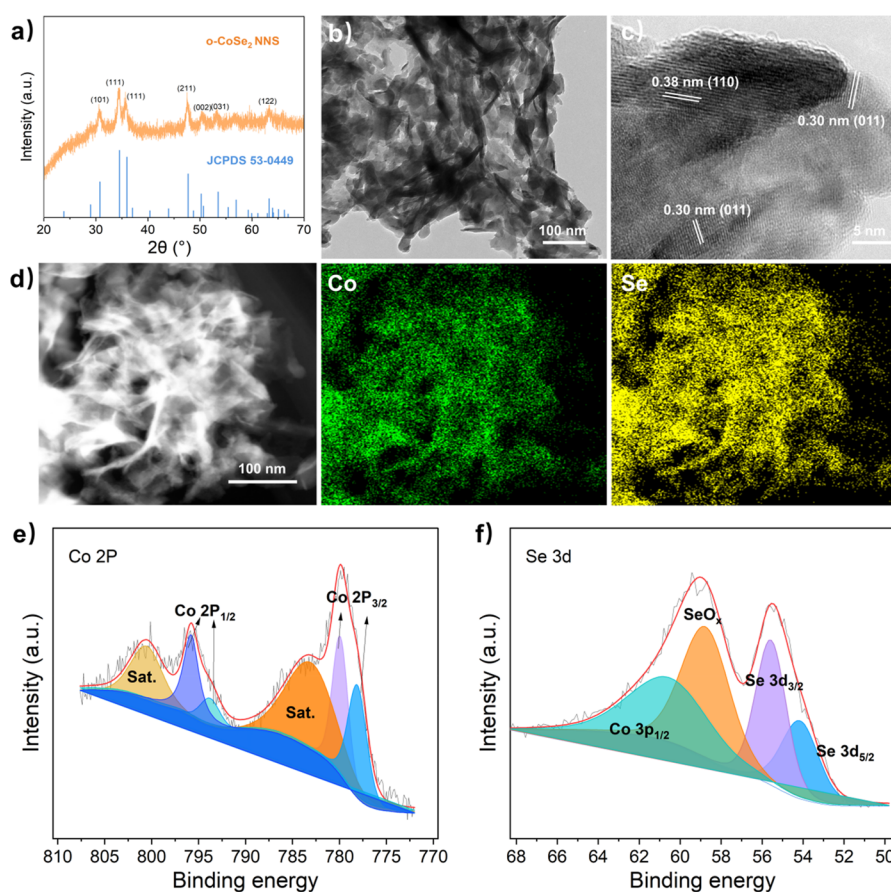**Figure 3.** (a) XRD patterns of o-CoSe$_2$ NNS and Co$_{0.85}$Se NNS, (b, c) TEM and HRTE images of o-CoSe$_2$ NNS (d) TEM image and the corresponding EDS element mappings of o-CoSe$_2$, (e, f) high-resolution XPS spectra of Co 3p and Se 3d of o-CoSe$_2$ NNS, respectively.

supposed to be convergent when the energy change was smaller than 0.05 eV Å^{-1}. The adsorption energies (E_{ads}) were calculated using the formula $E_{ads} = E_{ad/sub} − E_{ad} − E_{sub}$, where $E_{ad/sub}$, E_{ad}, and E_{sub} are the total energies of the optimized adsorbate/substrate system, the adsorbate in the gas phase, and the clean substrate, respectively. The free energies of elemental reaction steps were calculated by the computational hydrogen electrode model developed by Nørskov et al. The different free energies (ΔG) were calculated using the formula $\Delta G = \Delta E + \Delta E_{ZPE} − T\Delta S$, where ΔE, ΔE_{ZPE}, and ΔS are the binding

energy, the zero-point energy, and the entropy change, respectively.

3. RESULTS AND DISCUSSION

Flowerlike o-CoSe$_2$ NSS was prepared by the regeneration of flowerlike Co$_{0.85}$Se NSS through a heat treatment under an Ar atmosphere. Figure 1 shows the detailed synthesis process and its application in the alkaline hydrogen evolution reaction. First, ZIF-67 polyhedra were produced by a common synthetic method using Co^{2+} and 2-methylimidazole in an aqueous solution, as shown in Figures S1 and S2.[27] After that, a
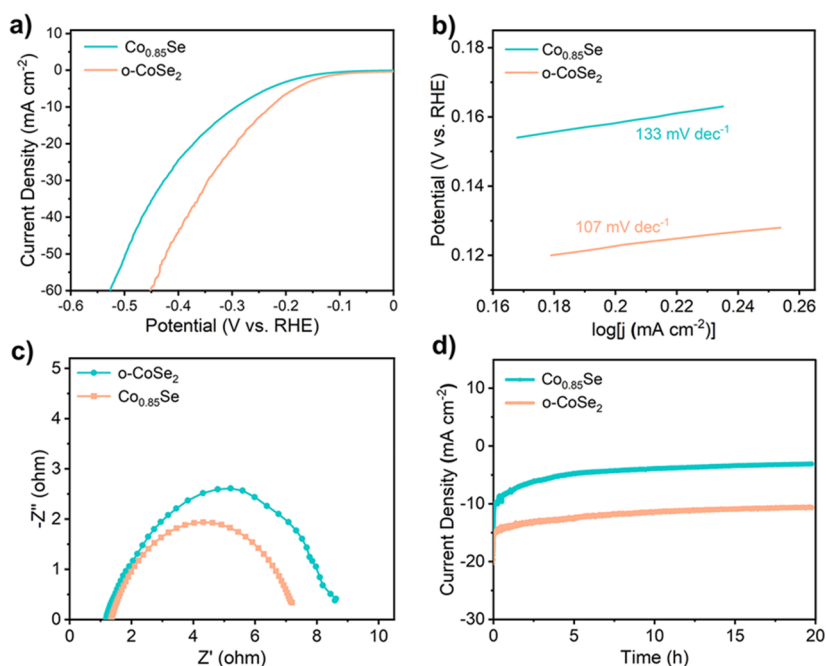
Figure 4. Electrochemical performance of $Co_{0.85}Se$ NNS and $o\text{-}CoSe_2$ NNS in 1 M KOH for the HER: (a) polarization curves; (b) Tafel plots; (c) Nyquist plots; (d) stability tests at a constant overpotential.

hydrothermal method was applied to synthesize $Co_{0.85}Se$ NSS by selenizing ZIF-67 polyhedra using Na_2SeO_3 as the selenium source. As shown in Figure 2a–c, the flower-like $Co_{0.85}Se$ material is approximately 1 μm in size and is composed of many nanosheets. Finally, $o\text{-}CoSe_2$ NSS was derived from $Co_{0.85}Se$ NSS, maintaining the original nanosheet structure well through calcination at 300 °C under an Ar atmosphere and there was no obvious change in size, as shown in Figure 2d–f. Furthermore, the electrocatalytic performances of $Co_{0.85}Se$ NSS and $o\text{-}CoSe_2$ NSS were measured in the alkaline hydrogen evolution reaction. To the best of our knowledge, this is a new and facile strategy for the synthesis of $o\text{-}CoSe_2$ in comparison with the typical selenization methods.[33−35]

XRD measurements were performed to characterize the crystalline structure of $o\text{-}CoSe_2$ and $Co_{0.85}Se$ for a confirmation of the structure transformation. As shown in Figure S3, before the calcination, the characteristic diffraction peaks at 33.1, 44.6, and 50.4° can be well indexed to the (101), (102), and (110) planes for $Co_{0.85}Se$ (JCPDS No. 52-1008; crystal structure shown in Figure 1) without any impurity peaks. The characteristic diffraction peaks observed in Figure 3a which are located at 30.7, 34.5, 35.9, and 47.7° correspond to the (011), (101), (111), (120) and (211) planes for the pure orthorhombic phase of $CoSe_2$ ($o\text{-}CoSe_2$, JCPDS No. 53-0445; crystal structure shown in Figure 1) after the calcination. This strongly suggests that $o\text{-}CoSe_2$ NNS is successfully transformed from $Co_{0.85}Se$ NNS after a calcination and the different ratios of Co and Se can probably be attributed to Se vacancies. The TEM image of $o\text{-}CoSe_2$ (Figure 3b) shows that $o\text{-}CoSe_2$ inherits the nanosheet structure of $Co_{0.85}Se$ (Figure S4a,b) well. Moreover, a high-resolution TEM (HRTEM) image of $Co_{0.85}Se$ (Figure S3c) only shows a set of lattice fringes corresponding to the (110) plane with an interplanar spacing of 0.18 nm, while the HRTEM image of $o\text{-}CoSe_2$ in Figure 3c exhibits two sets of obvious lattice fringes with interplanar spacings of 0.30 and 0.38 nm, which can be well ascribed to its (011) and (110) planes, respectively. The corresponding

energy dispersive spectrometry (EDS) element mapping images (Figure 3d and Figure S3d) of $o\text{-}CoSe_2$ and $Co_{0.85}Se$ clearly show the uniform distribution of Co and Se, respectively. On the basis of the above analysis, $o\text{-}CoSe_2$ NSS can be well transformed from the preprepared $Co_{0.85}Se$ NSS at a temperature of 300 °C, while the original nanosheet structure is maintained.

XPS was applied to investigate the elemental compositions and surface chemical states of $o\text{-}CoSe_2$ and $Co_{0.85}Se$ (Figure 3e,f and Figure S3e,f). As shown in Figure 3e, the high-resolution Co 2p spectrum consists of two pairs of spin−orbital peaks of Co^{3+} (778.9 eV for $2p_{3/2}$ and 794.6 eV for $2p_{1/2}$) and Co^{2+} (780.7 eV for $2p_{3/2}$ and 796.6 eV for $2p_{1/2}$), accompanied by two broad satellite peaks of Co $2P_{3/2}$ and Co $2p_{1/2}$.[26,36] Moreover, the peaks of an Se 3d spectrum in Figure 3f at 54.2 and 55.6 eV can be attributed to Se $3d_{5/2}$ and $3d_{3/2}$.[26,37] The remaining two peaks at 58.8 and 60.7 eV can be assigned to Co 3p and SeO_x, respectively.[26,36] The characterizations and analysis of XPS further demonstrate the successful preparation of $o\text{-}CoSe_2$. In addition, an XPS analysis of Co included in $Co_{0.85}Se$ was also performed, as shown in Figure S3e. The two sets of peaks of Co 2p corresponded to Co^{3+} (780.6 eV for $2p_{3/2}$ and 792.7 eV for $2p_{1/2}$) and Co^{2+} (779.8 eV for $2p_{3/2}$ and 795.7 eV for $2p_{1/2}$), respectively.[38,39] Then, the two broad peaks at 784.1 and 801.4 eV are attributed to satellite peaks similar to earlier reports.[38,39] The peaks of the Se 3d spectrum in Figure S3f at 54.1 and 55.1 eV can be attributed to Se $3d_{5/2}$ and $3d_{3/2}$, respectively.[40] The last two peaks at 58.7 and 60.4 eV are ascribed to Co 3p and SeO_x, respectively.[40]

The electrochemical performance of $Co_{0.85}Se$ and $o\text{-}CoSe_2$ NNS was determined to evaluate the electrocatalytic HER activities using a standard three-electrode system in an aqueous alkaline solution (1.0 M KOH, pH 14). Figure 4a shows the linear sweep voltammetry (LSV) polarization curves of $Co_{0.85}Se$ and $o\text{-}CoSe_2$ NNS, which are the typical characteristics to measure catalytic HER performance. A smaller
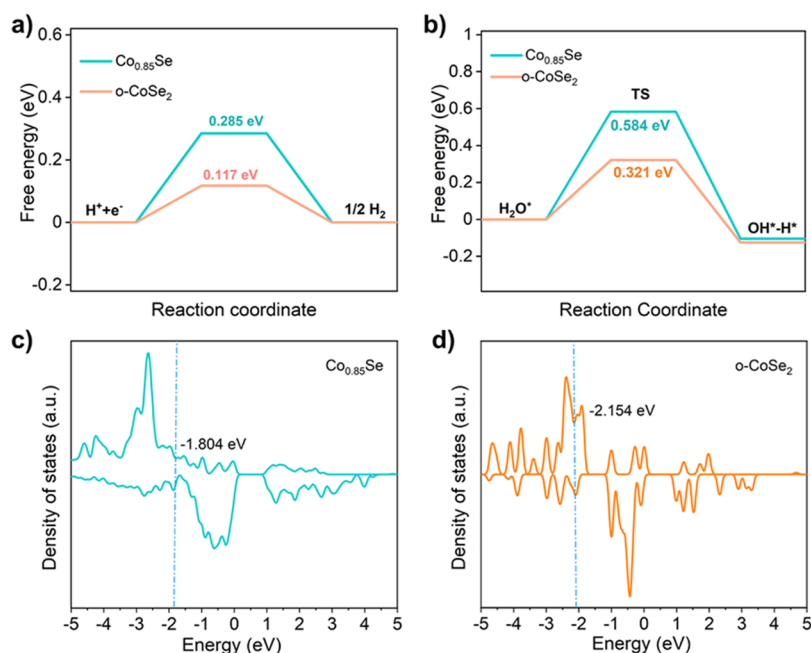
Figure 5. Theoretical calculations of o-CoSe$_2$ and Co$_{0.85}$Se: (a) free energy diagram for HER on Co sites; (b) calculated water adsorption energy on the surface of the catalysts; (c) the DOS of Co$_{0.85}$Se; (d) the DOS of o-CoSe$_2$.

overpotential of 220 mV for o-CoSe$_2$ in comparison to that of 286 mV for Co$_{0.85}$Se is required to reach the same current density of 10 mA cm^{-2}. The obtained corresponding Tafel slope calculated after linear fitting is 107 mV dec^{-1} for o-CoSe$_2$, which is obviously smaller than that of 133 mV dec^{-1} for Co$_{0.85}$Se (Figure 4b). The small Tafel slope is beneficial for practical applications as the overpotential increases slightly to achieve a greater current density. Hence, o-CoSe$_2$ has been confirmed to possess an enhanced alkaline HER activity in comparison with Co$_{0.85}$Se. EIS was used to characterize the electrocatalytic kinetics of interfacial charge transfer, and the charge transfer resistance (R_{ct}) was obtained from Nyquist plots, as shown in Figure 4c. A smaller R_{ct} value suggests an improved charge transfer ability along with superior electrode kinetics of o-CoSe$_2$ samples, which will induce faster electron transfer, further promoting the electrochemical HER activity. CV curves shown in Figure S5a,b were obtained at different scan rates to measure the double-layer capacitance C_{dl}, which is proportional to the ECSA. Obviously, the value of C_{dl} for o-CoSe$_2$ NNS (13.4 mF cm^{-2}) is larger than that of 2.5 mF cm^{-2} for Co$_{0.85}$Se NNS (Figure S5c). Clearly more active sites are exposed after the transformation of o-CoSe$_2$ from Co$_{0.85}$Se, which contribute to the superior HER activity. Continuous HER tests of o-CoSe$_2$ and Co$_{0.85}$Se NSS at a static overpotential were conducted (Figure 4d), which shows that the current density hardly changes after 20 h in an alkaline medium. In addition, the LSV curves of o-CoSe$_2$ and Co$_{0.85}$Se NSS before and after the stability tests also exhibit negligible changes (Figure S5d). Both of these results illustrate that the o-CoSe$_2$ NNS sample has excellent stability for the alkaline HER.

The enhanced HER performance of o-CoSe$_2$ NNS was further understood by correlating the intrinsic electronic structure and catalytic activity on the basis of density functional theory (DFT) calculations. Crucially, the effect of the o-CoSe$_2$ sample on the free energy of hydrogen (reaction intermediate) adsorption and the water adsorption energy was

studied, and their schematic models are displayed in Figures S6 and S7. ΔG_{H*} (the value of hydrogen Gibbs free energy) is the most important characteristic to evaluate the HER activity of the catalyst,[41,42] as the optimal HER activity of an electrocatalyst should have a ΔG_H value of around zero. It can be seen that the ΔG_{H*} of Co sites in o-CoSe$_2$ (0.117 eV) is much closer to the thermoneutral value (0) and smaller than that in Co$_{0.85}$Se (0.285 eV) from Figure 5a, suggesting the higher activity of o-CoSe$_2$, which is in good agreement with experimental HER results. In addition, the adsorption energy of an H$_2$O molecule (ΔG_{H_2O}) on the catalyst is the other important parameter to evaluate HER performance in alkaline solution (Figure 5b). ΔG_{H_2O} values for Co$_{0.85}$Se and o-CoSe$_2$ are 0.584 and 0.321 eV, respectively; the lower ΔG_{H_2O} value of o-CoSe$_2$ indicates that H$_2$O is more easily adsorbed and activated on the surface of o-CoSe$_2$ NNS to facilitate the HER process. Moreover, the density of states (DOS) of Co$_{0.85}$Se and o-CoSe$_2$ (Figure 5c,d) has also been calculated. The value of the d-band center of o-CoSe$_2$ is −2.154 eV, which is downshifted from the Fermi level in comparison with Co$_{0.85}$Se (−1.804 eV) after the regeneration. According to the d-band theory, a downshift of the d-band center will induce a weakening adsorption energy of H and accelerate the desorption of hydrogen on the catalyst surface, which is conducive to an improvement in HER activity.[43−48] In consideration of the theoretical investigations, o-CoSe$_2$ NNS derived from Co$_{0.85}$Se NNS tends to exhibit the expected result with a better HER activity, which is consistent with the electrocatalytic performance detailed above.

4. CONCLUSIONS

In summary, the temperature-induced structural transformation from Co$_{0.85}$Se NNS to o-CoSe$_2$ NNS has been reported. Such materials inherit the original nanosheet structure well after calcination. Importantly, o-CoSe$_2$ NNS possesses an enhanced HER performance with an overpotential of 220 mV

at 10 mA cm^{-2}. As expected, DFT studies also reveal that the d-band center downshift of o-CoSe$_2$ can promote an improvement in HER activity, which is consistent with the electrocatalytic test results. It is believed that our new findings in this work can facilitate the design and development of o-CoSe$_2$ as a highly efficient catalyst for the HER.

■ ASSOCIATED CONTENT

SI Supporting Information

The Supporting Information is available free of charge at https://pubs.acs.org/doi/10.1021/acsomega.2c01020.

XRD pattern, SEM images, TEM and HRTEM images, XPS spectra, CV curves, and schematic models (PDF)

■ AUTHOR INFORMATION

Corresponding Authors

Dongsheng Geng — *Beijing Advanced Innovation Center for Materials Genome Engineering, School of Material Science and Engineering, University of Science and Technology Beijing, Beijing 100083, People's Republic of China;* orcid.org/0000-0003-0910-8985; Email: dgeng@ustb.edu.cn

Dongjie Zhao — *Institute for Future, School of Automation, Qingdao University, Qingdao 266071, People's Republic of China;* Email: dongjiezhao@qdu.edu.cn

Authors

Jing Bai — *Beijing Advanced Innovation Center for Materials Genome Engineering, School of Material Science and Engineering, University of Science and Technology Beijing, Beijing 100083, People's Republic of China; Shunde Graduate School, University of Science and Technology Beijing, Foshan 528000, People's Republic of China;* orcid.org/0000-0002-9199-6602

Yechen Wang — *Beijing Advanced Innovation Center for Materials Genome Engineering, School of Material Science and Engineering, University of Science and Technology Beijing, Beijing 100083, People's Republic of China*

Yange Wang — *Beijing Advanced Innovation Center for Materials Genome Engineering, School of Material Science and Engineering, University of Science and Technology Beijing, Beijing 100083, People's Republic of China*

Tiantian Zhang — *Beijing Advanced Innovation Center for Materials Genome Engineering, School of Material Science and Engineering, University of Science and Technology Beijing, Beijing 100083, People's Republic of China*

Gang Dong — *Beijing Advanced Innovation Center for Materials Genome Engineering, School of Material Science and Engineering, University of Science and Technology Beijing, Beijing 100083, People's Republic of China*

Complete contact information is available at:
https://pubs.acs.org/10.1021/acsomega.2c01020

Notes

The authors declare no competing financial interest.

■ ACKNOWLEDGMENTS

■ REFERENCES

(1) Liu, X.; Zhang, X. Y.; Li, D. S.; Zhang, S. Q.; Zhang, Q. C. Recent advances in the "on-off" approaches for on-demand liquid-phase hydrogen evolution. *J. Mater. Chem. A* **2021**, *9*, 18164−18174.

(2) Liu, Y.; Kanhere, P. D.; Wong, C. L.; Tian, Y. F.; Feng, Y. H.; Boey, F.; Wub, T.; Chen, H. Y.; White, T. J.; Chen, Z.; Zhang, Q. C. Hydrazine-hydrothermal method to synthesize three-dimensional chalcogenide framework for photocatalytic hydrogen generation. *J. Solid State Chem.* **2010**, *183*, 2644−2649.

(3) Li, J.-z.; Ruan, Z.-h.; Zhu, L.; Li, Y.-d.; Xu, X.-z.; Yang, Y.-l.; Yuan, Y.; Lin, K.-f. Synergistic effect of K and I co-doped porous graphitic carbon nitride sphere for photocatalytic hydrogen evolution: experimental and theoretical study. *Sol. RRl.* **2021**, *5*, 2100292.

(4) Liu, X.; Zhang, T.-t; Li, Y.-d.; Zhang, J.; Du, Y.-c.; Yang, Y.-l.; Jiang, Y.-q.; Lin, K.-f. Construction of core-shell ZnS@In2S3 rhombic dodecahedron Z-scheme heterojunction structure: Enhanced photo-catalytic activity and mechanism insight. *Chem. Eng. J.* **2021**, *423*, 130138.

(5) He, T.-N.; Wang, W.-C.; Shi, F.-L.; Yang, X.-L.; Li, X.; Wu, J.-B.; Yin, Y.-D.; Jin, M.-S. Mastering the surface strain of platinum catalysts for efficient electrocatalysis. *Nat.* **2021**, *598*, 76−81.

(6) Wan, X.-K.; Wu, H.-B.; Guan, B.-Y.; Luan, D.-Y.; Lou, X.-W. Confining sub-nanometer Pt clusters in hollow mesoporous carbon spheres for boosting hydrogen evolution activity. *Adv. Mater.* **2020**, *32*, 1901349.

(7) Jiang, X.-L.; Jang, H.-S.; Liu, S.-G.; Li, Z.-J.; Kim, M.-G.; Li, C.; Qin, Q.; Liu, X.; Cho, J. The heterostructure of Ru$_2$P/WO$_3$/NPC synergistically promotes H$_2$O dissociation for improved hydrogen evolution. *Angew. Chem., Int. Ed.* **2021**, *60*, 4110−4116.

(8) Yan, Z.-H.; Sun, H.-M.; Chen, X.; Liu, H.-H.; Zhao, Y.-R.; Li, H.-X.; Xie, W.; Cheng, F.-Y.; Chen, J. Anion insertion enhanced electrodeposition of robust metal hydroxide/oxide electrodes for oxygen evolution. *Nat. Commun.* **2018**, *9*, 2373.

(9) Xue, N.; Lin, Z.; Li, P.-K.; Diao, P.; Zhang, Q.-F. Sulfur-doped CoSe$_2$ porous nanosheets as efficient electrocatalysts for the hydrogen evolution reaction. *ACS Appl. Mater. Interfaces* **2020**, *12*, 28288−28297.

(10) Zhang, S.-L.; Lu, X.-F.; Wu, Z.-P.; Luan, D.-Y.; Lou, X.-W. Engineering platinum-cobalt nano-alloys in porous nitrogen-doped carbon nanotubes for highly efficient electrocatalytic hydrogen evolution. *Angew. Chem., Int. Ed.* **2021**, *60*, 19068−19073.

(11) Wan, X.-K.; Wu, H.-B.; Guan, B.-Y.; Luan, D.-Y.; Lou, X.-W. Confining sub-nanometer Pt clusters in hollow mesoporous carbon spheres for boosting hydrogen evolution activity. *Adv. Mater.* **2020**, *32*, 1901349.

(12) Yan, H.-J.; Xie, Y.; Wu, A.-P.; Cai, Z.-C.; Wang, L.; Tian, C.-G.; Zhang, X.-M.; Fu, H.-G. Anion-modulated HER and OER activities of 3D Ni-V-based interstitial compound heterojunctions for high-efficiency and stable overall water splitting. *Adv. Mater.* **2019**, *31*, 1901174.

(13) Yu, J.; Li, W.-J.; Kao, G.-B.; Xu, C.-Y.; Chen, R.-R.; Liu, Q.; Liu, J.-Y.; Zhang, H.-S.; Wang, J. In-situ growth of CNTs encapsulating P-doped NiSe$_2$ nanoparticles on carbon framework as efficient bifunctional electrocatalyst for overall water splitting. *J. Energy Chem.* **2021**, *60*, 111−120.

(14) Ashwin Kishore, M.-R.; Larsson, K.; Ravindran, P. Two-dimensional CdX/C$_2$N (X = S, Se) heterostructures as potential photocatalysts for water splitting: a DFT study. *ACS Omega* **2020**, *5*, 23762−23768.

(15) Sun, Y.-Q.; Xu, K.; Wei, Z.-X.; Li, H.-L.; Zhang, T.; Li, X.-Y.; Cai, W.-P.; Ma, J.-M.; Fan, H.-J.; Li, Y. Strong electronic interaction in dual-cation-incorporated NiSe$_2$ nanosheets with lattice distortion for highly efficient overall water splitting. *Adv. Mater.* **2018**, *30*, 1802121.

(16) Feng, J.; Li, Q.; Wang, H.-J.; Zhang, M.; Yang, X.; Yuan, R.; Chai, Y.-Q. Hexagonal prism structured MnSe stabilized by nitrogen-

doped carbon for high performance lithium ion batteries. *J. Alloys Compd.* **2019**, *789*, 451−459.

(17) Hu, J.; Zhang, C.-X.; Zhang, Y.-Z.; Yang, B.-M.; Qi, Q.-L.; Sun, M.-Z.; Zi, F.-T.; Leung, M.-K.-H.; Huang, B.-L. Interface modulation of MoS₂/metal oxide heterostructures for efficient hydrogen evolution electrocatalysis. *Small* **2020**, *16*, 2002212.

(18) Che, H.-B.; Liu, X.-H.; Gao, Y.-F.; Liu, J.-R.; Cao, Z.-Z. Hydrothermal electrochemical deposition synthesis NiSe₂ as efficient counter electrode materials for dye-sensitized solar cells. *J. Alloys Compd.* **2017**, *705*, 645−651.

(19) Kong, D.-S.; Wang, H.-T.; Lu, Z.-Y.; Cui, Y. CoSe₂ nanoparticles grown on carbon fiber paper: an efficient and stable electrocatalyst for hydrogen evolution reaction. *J. Am. Chem. Soc.* **2014**, *136*, 4897.

(20) Liang, L.; Cheng, H.; Lei, F.-C.; Han, J.; Gao, S.; Wang, C.-M.; Sun, Y.-F.; Qamar, S.; Wei, S.-Q.; Xie, Y. Metallic single-unit-cell orthorhombic cobalt diselenide atomic layers: robust water-electrolysis catalysts. *Angew. Chem., Int. Ed.* **2015**, *54*, 12004.

(21) Chen, P.-Z.; Xu, K.; Tao, S.; Zhou, T.-P.; Tong, Y.; Ding, H.; Zhang, L.-D.; Chu, W.-S.; Wu, C.-Z.; Xie, Y. Phase-transformation engineering in cobalt diselenide realizing enhanced catalytic activity for hydrogen evolution in an alkaline medium. *Adv. Mater.* **2016**, *28*, 7527−7532.

(22) Zheng, Y.-R.; Wu, P.; Gao, M.-R.; Zhang, X.-L.; Gao, F.-Y.; Ju, H.-X.; Wu, R.; Gao, Q.; You, R.; Huang, W.-X.; Liu, S.-J.; Hu, S.-W.; Zhu, J.-F.; Li, Z.-Y.; Yu, S.-H. Doping-induced structural phase transition in cobalt diselenide enables enhanced hydrogen evolution catalysis. *Nat. Commun.* **2018**, *9*, 2533.

(23) Dai, J.-L.; Zhao, D.-K.; Sun, W.-M.; Zhu, X.-J.; Ma, L.-J.; Wu, Z.-X.; Yang, C.-H.; Cui, Z.-M.; Li, L.-G.; Chen, S.-W. Cu(II) ions induced structural transformation of cobalt selenides for remarkable enhancement in oxygen/hydrogen electrocatalysis. *ACS Catal.* **2019**, *9*, 10761−10772.

(24) Tuo, Y. X.; Wang, X. Y.; Chen, C.; Feng, X.; Liu, Z. Q.; Zhou, Y.; Zhang, J. Identifying the role of Ni and Fe in NiFe co-doped orthorhombic CoSe2 for driving enhanced electrocatalytic activity for oxygen evolution reaction. *Electrochim. Acta* **2020**, *335*, 135682.

(25) Jia, B. M.; Xue, Z. Q.; Liu, Q.; Liu, L. Q.; Liu, K.; Liu, M.; Chan, T.-S.; Li, Y. L.; Li, Z. J.; Su, C.-Y.; Li, G. Q. Hierarchical nanotubes constructed from CoSe2 nanorods with an oxygen-rich surface for an efficient oxygen evolution reaction. *J. Mater. Chem. A* **2019**, *7*, 15073−15078.

(26) Ding, H.; Xu, G. C.; Zhang, L.; Wei, B.; Hei, j.C.; Chen, L. A highly effective bifunctional catalyst of cobalt selenide nanoparticles embedded nitrogen-doped bamboo-like carbon nanotubes toward hydrogen and oxygen evolution reactions based on metal-organic framework. *J. Colloid Interface Sci.* **2020**, *566*, 296−303.

(27) Pan, Y.; Sun, K.-A.; Liu, S.-J.; Cao, X.; Wu, K.-L.; Cheong, W.-C.; Chen, Z.; Wang, Y.; Li, Y.; Liu, Y.-Q.; Wang, D.-S.; Peng, Q.; Chen, C.; Li, Y.-D. Core-shell ZIF-8@ZIF-67-Derived CoP nano-particle-embedded N-doped carbon nanotube hollow polyhedron for efficient overall water splitting. *J. Am. Chem. Soc.* **2018**, *140*, 2610−2618.

(28) Kresse, G.; Furthmüller, J. Efficiency of ab-initio total Energy calculations for metals and semiconductors using a plane-wave basis set. *Comput. Mater. Sci.* **1996**, *6*, 15−50.

(29) Kresse, G.; Furthmüller, J. Efficient iterative schemes for ab initio total-energy calculations using a plane-wave basis set. *Phys. Rev. B* **1996**, *54*, 11169−11186.

(30) Perdew, J.-P.; Burke, K.; Ernzerhof, M. Generalized gradient approximation made simple. *Phys. Rev. Lett.* **1996**, *77*, 3865−3868.

(31) Kresse, G.; Joubert, D. From ultrasoft pseudopotentials to the projector augmented-wave method. *Phys. Rev. B* **1999**, *59*, 1758−1775.

(32) Blöchl, P.-E. Projector Augmented-Wave Method. *Phys. Rev. B* **1994**, *50*, 17953.

(33) Zhu, Y.-P.; Chen, H.-C.; Hsu, C.-S.; Lin, T.-S.; Chang, C.-J.; Chang, S.-C.; Tsai, L.-D.; Chen, H.-M. Operando unraveling of the structural and chemical stability of p-substituted CoSe₂ electro-catalysts toward hydrogen and oxygen evolution reactions in alkaline electrolyte. *ACS Energy Lett.* **2019**, *4*, 987−994.

(34) Jia, B.-M.; Xue, Z.-Q.; Liu, Q.; Liu, Q.-L.; Liu, K.; Liu, M.; Chan, T.-S.; Li, Y.-L.; Li, Z.-J.; Su, C.-Y.; Li, G.-Q. Hierarchical nanotubes constructed from CoSe₂ nanorods with an oxygen-rich surface for an efficient oxygen evolution reaction. *J. Mater. Chem. A* **2019**, *7*, 15073−15078.

(35) Zhang, H.; Wang, T.-T.; Sumboja, A.; Zang, W.-J.; Xie, J.-P.; Gao, D.-Q.; Pennycook, S.-J.; Liu, Z.-L.; Guan, C.; Wang, J. Integrated hierarchical carbon flake arrays with hollow P-doped CoSe₂ nanoclusters as an advanced bifunctional catalyst for Zn-air batteries. *Adv. Funct. Mater.* **2018**, *28*, 1804846.

(36) Zhang, Y.-F.; Pan, A.-Q.; Wang, Y.-P.; Cao, X.-X.; Zhou, Z.-L.; Zhu, T.; Liang, S.-Q.; Cao, G.-Z. Self-templated synthesis of N-doped CoSe₂/C double-shelled dodecahedra for high-performance super-capacitors. *Energy Storage Mater.* **2017**, *8*, 28−34.

(37) Meng, J.-S.; Niu, C.-J.; Xu, L.-H.; Li, J.-T.; Liu, X.; Wang, X.-P.; Wu, Y.-Z.; Xu, X.-M.; Chen, W.-Y.; Li, Q.; Zhu, Z.-Z.; Zhao, D.-Y.; Mai, L.-Q. General oriented formation of carbon nanotubes from metal-organic frameworks. *J. Am. Chem. Soc.* **2017**, *139*, 8212−8221.

(38) Shen, S.-J.; Lin, Z.-P.; Song, K.; Wang, Z.-P.; Huang, L.-G.; Yan, L.-H.; Meng, F.-Q.; Zhang, Q.-H.; Gu, L.; Zhong, W.-W. Reversed active sites boost the intrinsic activity of graphene-like cobalt selenide for hydrogen evolution. *Angew. Chem., Int. Ed.* **2021**, *60*, 12360−12365.

(39) Liu, Z.-W.; Han, K.; Li, P.; Wang, W.; He, D.-L.; Tan, Q.-W.; Wang, L.-Y.; Li, Y.; Qin, M.-L.; Qu, X.-H. Tuning metallic Co₀.₈₅Se quantum dots/carbon hollow polyhedrons with tertiary hierarchical structure for high-performance potassium ion batteries. *Nano-Micro Lett.* **2019**, *11*, 96.

(40) Li, X. F.; Pan, D.; Deng, J.; Wang, R.; Huang, J. Z.; Lü, W. M.; Yao, T.; Wang, X. J.; Zhang, Y. M.; Xu, L. L.L; Bai, Y.; Xu, P.; Song, B. Phase-junction engineering boosts the performance of CoSe 2 for efficient sodium/potassium storage. *J. Mater. Chem. A* **2021**, *9*, 25954−25963.

(41) Hu, J.-S.; Duan, W.-Y.; He, H.; Lv, H.; Huang, C.-Y.; Ma, X.-G. A promising strategy to tune the schottky barrier of a MoS₂₍₁₋ₓ₎Se₂ₓ/graphene heterostructure by asymmetric Se doping. *J. Mater. Chem. C* **2019**, *7*, 7798−7805.

(42) Jing, S.-Y.; Lu, J.-J.; Yu, G.-T.; Yin, S.-B.; Luo, L.; Zhang, Z.-D.; Ma, Y.-G.; Chen, W.; Shen, P.-K. Carbon-encapsulated WOₓ hybrids as efficient catalysts for hydrogen evolution. *Adv. Mater.* **2018**, *30*, 1705979.

(43) Ge, Y.-C.; Dong, P.; Craig, S.-R.; Ajayan, P.-M.; Ye, M.-X.; Shen, J.-F. Transforming nickel hydroxide into 3D prussian blue analogue array to obtain Ni₂P/Fe₂P for efficient hydrogen evolution reaction. *Adv. Energy Mater.* **2018**, *8*, 1800484.

(44) Zhou, Q.-W.; Shen, Z.-H.; Zhu, C.; Li, J.-C.; Ding, Z.-Y.; Wang, P.; Pan, F.; Zhang, Z.-Y.; Ma, H.-X.; Wang, S.-Y.; Zhang, H.-G. Nitrogen-doped CoP electrocatalysts for coupled hydrogen evolution and sulfur generation with low energy consumption. *Adv. Mater.* **2018**, *30*, 1800140.

(45) Yang, C.-M.; Wang, C.-T.; Zhou, L.-H.; Duan, W.; Song, Y.-Y.; Zhang, F.-C.; Zhen, Y.-Z.; Zhang, J.-J.; Bao, W.-W.; Lu, Y.-X.; Wang, D.-J.; Fu, F. Refining d-band center in Ni₀.₈₅Se by Mo doping: a strategy for boosting hydrogen generation via coupling electrocatalytic oxidation 5-hydroxymethylfurfural. *Chem. Eng. J.* **2021**, *422*, 130125.

(46) Liu, W.; Geng, P.; Li, S.-Q.; Liu, W.-H.; Fan, D.-Y.; Lu, H.-D.; Lu, Z.-H.; Liu, Y.-P. Tuning electronic configuration of WP₂ nanosheet arrays via nickel doping for high-efficiency hydrogen evolution reaction. *J. Energy Chem.* **2021**, *55*, 17−24.

(47) Wang, L.; Li, Z.-J.; Wang, K.-X.; Dai, Q.-Z.; Lei, C.-J.; Yang, B.; Zhang, Q.-H.; Lei, L.-C.; Leung, M.-K.-H.; Hou, Y. Tuning d-band center of tungsten carbide via Mo doping for efficient hydrogen evolution and Zn-H₂O cell over a wide pH range. *Nano Energy* **2020**, *74*, 104850.

(48) Chen, Z.-Y.; Song, Y.; Cai, J.-Y.; Zheng, X.-S.; Han, D.-D.; Wu, Y.-S.; Zang, Y.-P.; Niu, S.-W.; Liu, Y.; Zhu, J.-F.; Liu, X.-J.; Wang, G.-M. Tailoring the d-band centers enables Co₄N nanosheets to be

highly active for hydrogen evolution catalysis. *Angew. Chem., Int. Ed.* **2018**, *57*, 5076−5080.